



## The Renewable of Low Toxicity Gelcasting Porous Ceramic as Fe<sub>2</sub>O<sub>3</sub> Catalyst Support on Phenol Photodegradation

Suriati Eka Putri<sup>1\*</sup>, Diana Eka Pratiwi<sup>1</sup>, Rachmat Triandi Tjahjanto<sup>2</sup>, Hasri<sup>1</sup>, Irhamsyah Andi<sup>3</sup>, Abd Rahman<sup>1</sup>, Andi Indra Wulan Sari Ramadani<sup>4</sup>, Anita Nur Ramadhani<sup>5</sup>, Subaer<sup>3</sup>, Ahmad Fudholi<sup>6</sup>

<sup>1</sup> Department of Chemistry, Universitas Negeri Makassar, Jalan Daeng Tata Raya, Makassar 90244, Indonesia

<sup>2</sup> Department of Chemistry, Brawijaya University, Jalan Veteran, Malang 65145, Indonesia

<sup>3</sup> Department of Physics, Universitas Negeri Makassar, Jalan Daeng Tata Raya, Makassar 90244, Indonesia

<sup>4</sup> Department of Physics, Gorontalo University, Jalan Jenderal Sudirman, Gorontalo 96211, Indonesia

<sup>5</sup> Department of Chemistry, Indonesia University, Jalan Margonda Raya, Depok 16424, Indonesia

<sup>6</sup> Solar Energy Research Institute, Universiti Kebangsaan Malaysia, Selangor 43600, Malaysia

Corresponding Author Email: [ekaputri\\_chem@unm.ac.id](mailto:ekaputri_chem@unm.ac.id)

<https://doi.org/10.18280/ijdne.170403>

### ABSTRACT

**Received:** 20 March 2022

**Accepted:** 6 June 2022

#### Keywords:

*cassava starch, natural clay, catalyst reuse, phenol, photodegradation*

Low toxicity gelcasting water-based method was conducted using a non-acrylamide system, with cassava starch and natural clay as poregenic agent and raw material, respectively, and the resulting porous ceramic was used as Fe<sub>2</sub>O<sub>3</sub> catalyst support. The concentrations of cassava starch used were 1%, 3%, 5%, 7%, and 9%, the sintering process was performed based on the results of TGA/DTA thermal analysis. In addition, the sol-gel coating method was used to impregnate the Fe<sub>2</sub>O<sub>3</sub> catalyst into the porous ceramic. BET results show that the pores formed in the ceramic body are micro pores with a size range of 21.41-23.27 Å, hence the concentration of cassava starch does not affect the pore characteristics. The morphology of SEM results also indicated the presence of pore formation in the ceramic body. According to the quantitative XRD analysis, the cassava concentration affects the percentage of catalyst impregnated. The highest percentage of Fe<sub>2</sub>O<sub>3</sub> catalyst on 7% cassava starch was 41.15% and the phase of the catalyst successfully impregnated was α-Fe<sub>2</sub>O<sub>3</sub> with a rhombohedral structure. In addition, the highest percentage of phenol degradation was 59.15% with good performance after 8 times of recycling. In this study, we provide for the first time, utilization of Fe<sub>2</sub>O<sub>3</sub>-porous ceramics with a wonderful performance of recycling ability in the process of phenol photodegradation.

## 1. INTRODUCTION

Water pollution of organic compounds has harmful effects on aquatic life and human life, so reducing organic compound pollutants is very important. One of the organic compounds found in water is phenol, a harmful compound found in wastewater that requires specific attention [1] as indicated by the United States Environmental Protection Agency (EPA) [2] due to its severe risk to human health at very low concentrations. Therefore, several international regulatory authorities, such as the EPA [3], have imposed restrictions on phenol concentration in wastewater, which should not exceed 1 part per billion (ppb). The exposure of wastewater to phenol contents of 9-15 mg/L causes major health concerns.

Generally, techniques such as biodegradation, physical separation, and oxidation are used utilized in wastewater treatment to remove pollutants [4-7]. The degradation of phenol using Fenton catalyst was performed using CuNiSn LDHs which successfully degraded 97.8% of phenol [8]. However, the photocatalytic degradation method using MgAlSn hydroxalcite degraded phenol by 80% [9]. This study used the photodegradation method to reduce the phenol levels in the solution.

The catalyst used in this study is Fe<sub>2</sub>O<sub>3</sub>, which has been used

previously with a peroxymonosulfate activator to achieve a phenol degradation percentage of 97.6% [10]. Also, the photocatalyst is supported in porous materials, such as kaolin [11], clay [12-15], and zeolites [16], to increase the catalytic activity. This study used a porous ceramic as catalyst support because powdered catalyst has low reproducibility. Studies of [17] on the use of porous ceramics as catalyst support are conducted due to their great repeatability and catalytic efficacy of the impregnated catalysts.

Several techniques have been used for porous ceramics fabrication, including dip coating [18], extrusion [19], injection molding [20], tape casting [21], and the slip casting [22] process. This approach has some drawbacks, including being difficult to make, needing high pressure, and necessitating the use of a porous template [23]. The gelcasting method is a well-known and straightforward method than the others and involves in situ polymerization in the slurry [23-25]. Also, the distributed polymer serves as a binder and pore template when released during the sintering process, and polyacrylamide is the commonly used polymer [20-22]. There have been studies on the fabrication of gelcasting porous ceramics using natural clay as raw material and acrylamide (AM) as a monomer with methylene bisacrylamide (MBAM) crosslinker [26]. However, these polymers are toxic [27],

hence, alternatives are required to produce eco-friendly porous gelcasting ceramics. Some natural ingredients that are proposed as binders include starch [27-29], rice flour [30], egg white protein [31], and glutaraldehyde [32].

In this study, the cassava starch was used as polymer, while the natural clay was used as raw material. Furthermore, the starch forms a cross-linked gel and immobilizes the clay powders into the desired shape [33], hence, the use of starch as a pore-forming agent does not require a gelling agent. The pores are formed in the ceramic body through the degradation of cassava starch in the sintering stage [34]. It indicates that the use of cassava starch minimizes the use of chemicals in the gelcasting process of fabricating porous ceramics, though there are no report on this method of low toxicity.

## 2. MATERIALS AND METHODS

### 2.1 Materials

The raw material used to prepare low toxicity gelcasting porous ceramic samples was similar to previous work [24, 31, 32, 35, 36]. Carboxymethyl cellulose (CMC) (ex Perancis Ashland France Blanose) was used as dispersant. Cassava starch extracted according to the procedure described by Pepper et al. [37]. Cassava starch acted as gelifying agents and porogenic agents.

### 2.2 Pre-treatment of natural clay

The raw natural clay was ground and sieved using a 60 mesh sieve and produced approximately 60 mesh or 250 microns sieved clay. Then the sieved clay was extracted using 3M H<sub>2</sub>SO<sub>4</sub> at 80°C to dissolve impurities in the form of iron with high content in clay [38]. Furthermore, the element compositions of natural clay before and after extraction, as the metal oxides formation, are represented from the XRF measurement and shown in Table 1.

The XRF measurement of the raw and treated natural clay using Thermo Fisher Scientific's XRF with x-ray path: air, with Eff. Stationary and Area of 13.0 mm and 132.7 mm<sup>2</sup>.

**Table 1.** The composition of metal oxide on natural clay using XRF

Element	Composition (%weight)	
	Before extraction	After extraction
SiO <sub>2</sub>	66.12	73.15
Al <sub>2</sub> O <sub>3</sub>	14.30	14.14
Fe <sub>2</sub> O <sub>3</sub>	9.98	5.32
TiO <sub>2</sub>	1.89	0.78
K <sub>2</sub> O	1.44	1.31
MnO	1.35	1.02
CaO	1.24	1.15
ZrO <sub>2</sub>	0.94	0.75
Cr <sub>2</sub> O <sub>3</sub>	0.49	0.34
NiO	0.43	0.39
CuO	0.72	0.74
SrO	0.81	0.79
ZnO	0.29	0.12

### 2.3 Synthesis low toxicity gelcasting porous ceramic

5 g of natural clay and 0.1 g of CMC were added to distilled water in a ratio of 50:1 (50% vol) [23]. Then, the aqueous

suspension was added cassava starch with various concentrations of 1, 3, 5, 7, and 9 wt% [28]. The gelation time was measured by flipping 15 mm diameter and 120 mm long glass tube with 5 mL solution until gelation occurred. The gelation was completed when the product inside the tube did not move at all when the tube position was reversed [39]. The results shows that the higher concentration of cassava starch, the lower gelation time. This condition was correlated with the slurry viscosity that influenced the particles collision. Ultimately, the gel formation will be achieved faster.

It indicates that the possibly of the affect of cassava starch concentration to the characteristics of porous ceramics It indicates that the possibly of the affect of cassava starch concentration to the characteristics of porous ceramics.

Furthermore, the ball-milled suspension was poured into a PVC mold of 25x25x120 mm<sup>3</sup>, allowed to gel at room temperature for 12 hours, and dried. The gelcasted green body ceramic was sintered with a heating rate based on thermal analysis results.

### 2.4 Determination of sintering temperature

Determination of sintering temperature from thermal analysis of Thermogravimetric (TG) and differential thermal (DTA) analysis Hitachi STA7300 was carried out simultaneously. About 6.864 mg of gelcasted green body ceramic was weighed on an alumina crucible and isothermally heated at 30°C for 10 minutes under airflow (8 L/min) and then heated to 1100°C in a static air atmosphere. The heating rate was 30°C/min, and the alumina was used as the reference material. This was performed at 1100°C at a rate of 50°C per 30 minutes, with temperature holding at 100°C, 300°C, 500°C, 600°C, and 1100°C for 1 hour.

### 2.5 Impregnation Fe<sub>2</sub>O<sub>3</sub> catalyst

Figure 1 depicts the illustration of impregnation Fe<sub>2</sub>O<sub>3</sub> catalyst into gelcasting porous ceramic by coating sol-gel method. Firstly, the NH<sub>4</sub>OH solution was added (NH<sub>4</sub>)<sub>2</sub>SO<sub>4</sub> in a ratio of 1:1 (v/v) to make a mixture solution, then FeCl<sub>3</sub> was added into the mixture solution in ratio 1:5 (w/v), and the solution was stirred for 6 hours at a temperature of 85°C. Furthermore, all of porous ceramic body was dipped into the mixture solution in ratio 1:10 (w/v) while stirring for 5 hours, and then the prepared ceramic was moved out from the solution furthermore, the wet ceramic was dried at a temperature of 60°C overnight, and followed by the calcination with a temperature of 600°C for 3 hours.

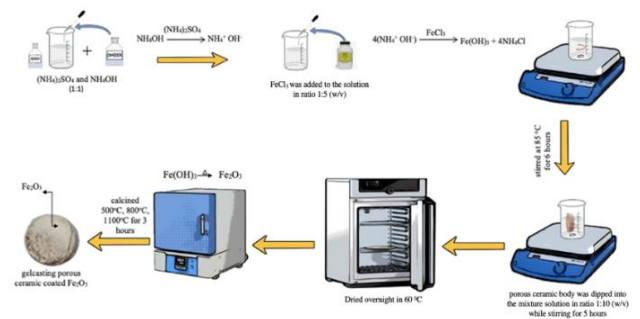


**Figure 1.** The illustration of impregnation Fe<sub>2</sub>O<sub>3</sub> catalyst into gelcasting porous ceramic by coating sol-gel method

## 2.6 Sample characterization

The structural phase parameters of Fe<sub>2</sub>O<sub>3</sub>/porous ceramic were analyzed using a quantitative analysis of XRD spectroscopy (Shimadzu 7000) with CuK $\alpha$  radiation ( $\lambda = 1.5405 \text{ \AA}$ ) ranging from  $15^\circ \leq 2\theta \leq 80^\circ$ , and operation at 30 kV and 10 mA. The morphology of prepared Fe<sub>2</sub>O<sub>3</sub>/Porous ceramic was determined by the SEM analysis.

The pore volume and pore radius of the gelcasting porous ceramic was determined by adsorption N<sub>2</sub> using surface area analyzer type Quantachrome Nova 4200e with outgas time of 3 hours at a temperature of 250°C and bath temperature of 273 K. The specific textural properties as the surface area and the pore volume were calculated by T-Plot method with the total pore volume was represented by the total adsorbed gas at relative pressure  $P/P_0 = 0.99$ , then for the pore distribution based on BJH analysis.

## 2.7 Phenol photodegradation

Phenol photodegradation was evaluated under UV irradiation with a 100 W halogen lamp in a cylindrical reactor with constant mechanical stirring at 23°C. The gelcasting porous ceramic coating Fe<sub>2</sub>O<sub>3</sub> was placed in the column containing 25 mL of 10 mg/L phenol solution with a pH 8 and irradiated time of 3 hours, this condition based on the optimum results of Mohamed et al. [40]. A Shimadzu UV-Vis spectrophotometer was used to test the results of the phenol photodegradation at a wavelength 316 nm. The recycle test measured by the stability of photocatalytic properties Fe<sub>2</sub>O<sub>3</sub>-porous ceramic was tested by repetition of phenol photodegradation with the use of the same sample (which have the highest degradation percentage) under the same experimental conditions.

## 3. RESULTS AND DISCUSSION

The high content of alumina and silica in natural clay indicated that it can be used as raw material for ceramic fabrication [41]. Meanwhile, the low toxicity water-based gelcasting was used in the fabrication of porous ceramics, using cassava starch and natural clay as a porogenic agents and raw material, respectively. Therefore, a thermal study to determine the degradation temperature of starch polymers is necessary to form pores in the ceramic body. The pattern of thermal analysis is based on the changes of the mass sample during the increasing rate of temperature, which the increasing heat interval is 30°C/min.

The thermal analysis results of the gelcasted green body ceramic were used to determine the sintering temperature. The results showed there are three stage of weight loss during heating were observed (Figure 2). The first stage occurs between 25°C and 180°C with weight loss of 5.49% likely due to the release of associated H<sub>2</sub>O and removal of free and physically adsorbed water on the surface of the piece and in the starch consolidation, as also reported by Calado et al. [42]. The second stage correspond to 8.15% of weight loss and occurs at a temperature between 260°C and 310°C possibly due to the thermal decomposition of starch begins and continues in the third step with oxidative decomposition. The third stage occurs between 400°C and 550°C with weight loss of 12.8% possibly due to carbon dioxide released by the degradation of the starch polymer and the release of the

hydroxide group from aluminum hydroxide to alumina, respectively [43]. According to Talou and Camerucci [44] the total degradation of starch occurs in the temperature range of 250°C to 550°C.

Besides that the DTA results showed at a temperature of 500°C as demonstrated by the appearance of a down peak, indicating the rearrangement of metal oxides to become denser, hence an exothermic peak appears after a temperature of 500°C. Furthermore, a gentle DTA curve is observed at temperatures between 600°C to 1000°C, which is associated with the phase transformation from meta kaolinite to Al-Si spinel [45].

The pore characteristic in the gelcasting ceramics body was illustrated by BET analysis. The nitrogen adsorption-desorption isotherms and their corresponding pore distributions of gelcasting porous ceramics with varying concentrations of cassava starch before and after impregnation, shown in Figure 3. and the corresponding of pore structure properties (the specific surface area, total pore volume, and average pore diameter) are shown in Table 2. It was determined using the nitrogen adsorption-desorption isotherms, and the pore character of the ceramic body is not affected by the cassava starch concentration. According to the Brunauer-Deming-Deming-Teller classification, the adsorption isotherms for gelcasting porous ceramic of the cassava starch concentration are close to type V, indicating that weak interaction between gas and solid can occur in microporous or mesoporous solids. In addition, type V adsorption isotherm occurs in polar and non-polar molecules [46].

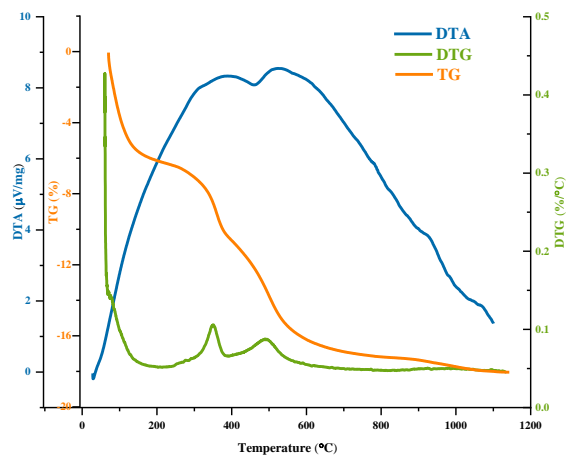


**Figure 2.** Thermal analysis of gelcasted green body ceramic using TGA/DTA

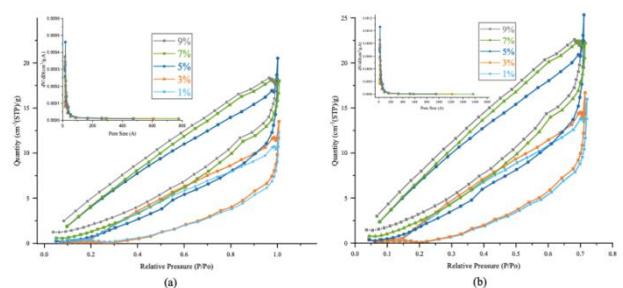


**Figure 3.** The Brunauer-Emmett-Teller (BET), nitrogen adsorption isotherms of quantity adsorbed against the relative pressure of N<sub>2</sub>, for porous ceramic and pore size distributions (inserted), (a) before impregnated and (b) after impregnated

**Table 2.** Pore structure properties of gelcasting porous ceramic with variation of cassava starch concentration before and after catalyst impregnated

Sample (Cassava starch concentration)	$S_{BET}$ ( $m^2/g$ )		$V_t$ ( $cm^3/g$ )		Average Pore Diameter ( $\text{\AA}$ )	
	Before impregnated	After impregnated	Before impregnated	After impregnated	Before impregnated	After impregnated
1%	13.17	19.18	0.0042	0.0035	21.41	21.26
3%	18.16	21.41	0.0078	0.0076	21.63	21.41
5%	20.12	23.74	0.0081	0.0079	22.13	21.76
7%	34.57	31.92	0.0114	0.0107	23.27	23.19
9%	39.41	41.09	0.0119	0.0109	23.19	22.86

**Table 3.** Crystallinity, average crystallite size, and percentage of  $Fe_2O_3$  determined from the quantitative analysis of XRD spectra (Figure 5) of  $\alpha-Fe_2O_3$  impregnated on porous ceramic

Cassava starch concentration of porous ceramic	Crystallinity (%)	Average crystallite size (nm)	Percentage of $\alpha-Fe_2O_3$ (%)
1%	41.56	21.42	38.52
3%	42.02	22.78	37.98
5%	43.72	23.81	37.83
7%	38.97	19.97	41.15
9%	39.18	20.14	37.62

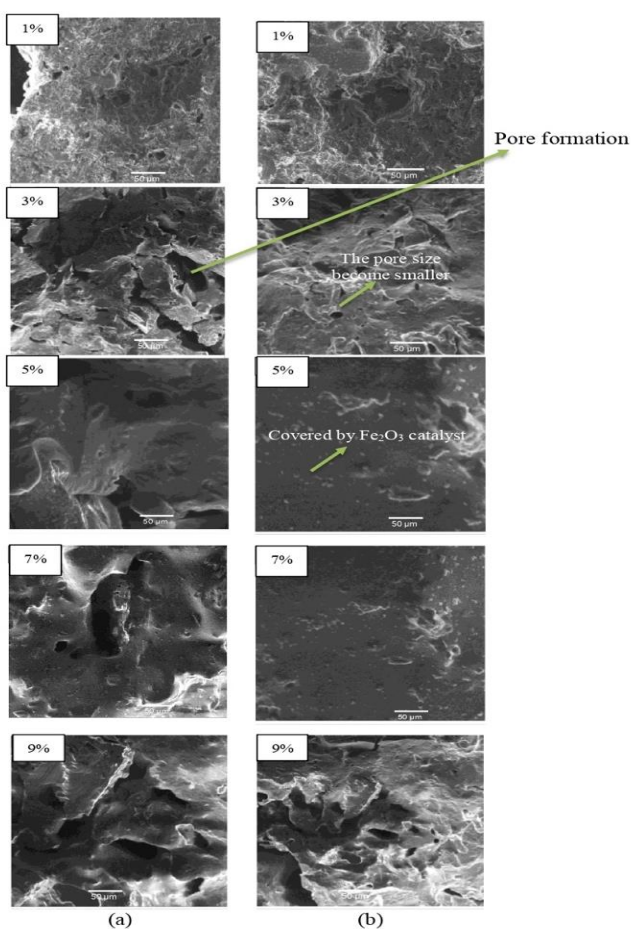


**Figure 4.** The morphology of gelcasting porous ceramic, (a) before catalyst impregnated and (b) after catalyst impregnated

The resulting pore size was microporous, the research before [47] reported that the catalyst distribution improves porous surfaces with microporous sizes, allowing the gelcasting porous ceramic to be used as  $Fe_2O_3$  catalyst support. Table 2. shows the successful impregnation of catalysts into the porous ceramic bodies, where the increased surface area and decreased pore volume indicate the presence of catalysts

that have occupied the pores, and this is in line with the results of Alamdari, and Karimzadeh [48].

The pore formation in the ceramic body as observed in the results of the morphological analysis of the ceramic body using SEM, shown in Figure 4. The surface of the ceramic body after impregnation depicts the morphology of the ceramic with the smaller pore shape indicating that they are covered by  $Fe_2O_3$  catalyst. This is related with pore structure properties, the value of  $V_t$  and the average pore diameter decrease after impregnation, which is shown in Table 2. The table informs that the impregnation process influences this decrease phenomenon mainly due to solid metal species at the pores [49].

Ceramics coating are currently being developed by several researchers for several applications [50]. The coating sol-gel method was used to impregnate the  $Fe_2O_3$  catalyst analysis into the gelcasting porous ceramic body as shown in Figure 5, which the  $Fe_2O_3$  phase impregnated is  $\alpha-Fe_2O_3$ . The XRD patterns of the  $\alpha-Fe_2O_3$  structure showed major peaks at  $2\theta = 33.1, 35.6, 50.1,$  and  $55.1^\circ$  which correspond to the 104, 110, 024, and 116, respectively, of  $\alpha-Fe_2O_3$ . The diffraction peaks of the samples were found to correspond to the rhombohedral  $\alpha-Fe_2O_3$  (PDF Number 84-0307), with  $a = b = 5.035 \text{ \AA}$  and  $c = 13.742 \text{ \AA}$ .

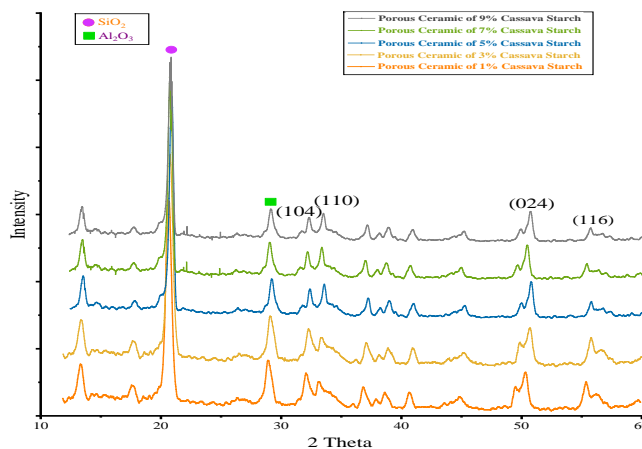


**Figure 5.** The XRD spectra of gelcasting porous ceramic impregnated  $Fe_2O_3$

The impregnation of the quantitative analysis of  $\alpha$ -Fe<sub>2</sub>O<sub>3</sub> catalyst into gelcasting porous ceramic body using coating sol-gel method with variations cassava starch concentration, shown in Table 3. The crystallinity of the material and the average crystallite size were similar for each variation in the cassava starch concentration, while the largest percentage of  $\alpha$ -Fe<sub>2</sub>O<sub>3</sub> was 41.15%, occurring at a concentration of 7% due to the type of pore formed. According to the SEM results in Figure 4, the type of pore formed in the 7% ceramic body is an open pore, hence the catalyst impregnation process can take place optimally [45]. In addition, the  $\alpha$ -Fe<sub>2</sub>O<sub>3</sub> phase was used as a catalyst in previous studies, including azo dyes degradation [4], NO<sub>x</sub> gas reduction [51], and CO oxidation [52].

The effectiveness of the photodegradation process is seen from the concentration of the degraded phenol expressed in percent (%) in Eq. (1):

$$\%E = \frac{C_a - C_s}{C_a} \times 100\% \quad (1)$$

where,  $C_a$  is the initial concentration of phenol and  $C_s$  is the final concentration of phenol after photodegradation using  $\alpha$ -Fe<sub>2</sub>O<sub>3</sub>-porous ceramic. Figure 6 illustrates the results of phenol degradation using Fe<sub>2</sub>O<sub>3</sub>-porous ceramic.

The highest phenol photodegradation was 59.15%, occurring in the 7% cassava starch concentration (Figure 6). This high percentage is related to the percentage of catalysts that have been impregnated, where porous ceramics with 7% cassava starch had the highest amount of Fe<sub>2</sub>O<sub>3</sub> catalyst (Table 3). Figure 6(b) demonstrated the effectiveness of  $\alpha$ -Fe<sub>2</sub>O<sub>3</sub>-porous ceramic, which the control sample was not degraded due to the absence of photon energy from UV lights and photocatalysts that generate hydroxyl radicals. However, the process had a percentage degradation of 18.37% using only UV due to the occurrence of water photolysis reactions, particularly the decomposition of H<sub>2</sub>O molecules after absorbing photons (hv) from UV lights to produce  $\bullet$ OH, H<sup>+</sup> and electrons. The  $\bullet$ OH produced is relatively low, hence, the reaction proceeds slowly [53]. Meanwhile, the percentage of phenol degradation that only uses porous ceramics was 11.76% because only the adsorption process occurs, though there is an increase of 21.79% with the addition of UV light. The use of UV may cause the Fenton photo process to occur because the Fe element contained in natural clay forms hydroxyl radicals, which attack phenolic compounds [54].

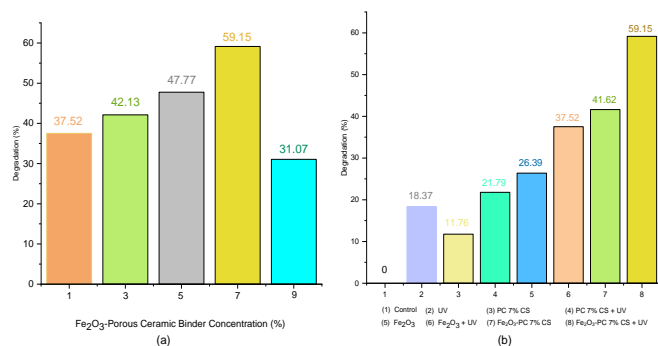
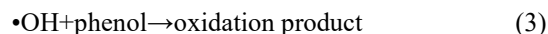


**Figure 6.** Phenol photodegradation (a) various cassava starch concentration (b) effectiveness of  $\alpha$ -Fe<sub>2</sub>O<sub>3</sub>-porous ceramic

The mechanism shown in Eq. (2) and (3):



The degradation using only  $\alpha$ -Fe<sub>2</sub>O<sub>3</sub> catalyst was 26.39% and it increased by 37.52% on the addition of UV light, indicating a photodegradation reaction. The Fe<sub>2</sub>O<sub>3</sub> irradiated by UV light causes the excitation of electrons from the valence to the conduction band, and the displaced electrons leave a positively charged hole. The presence of water vapor in the hole causes the formation of  $\bullet$ OH, while the electrons in the conduction band interact with O<sub>2</sub> to produce O<sub>2</sub><sup>-</sup>. These radicals and ions are very reactive, hence, they degrade phenolic compounds into CO<sub>2</sub> and H<sub>2</sub>O. Figure 7 shows the mechanism of phenol photodegradation by  $\alpha$ -Fe<sub>2</sub>O<sub>3</sub> catalyst impregnated on gelcasting porous ceramic and Figure 8 illustrates the schematic of catalyst activity in degrading phenol.

The next treatment used a porous ceramic impregnated with Fe<sub>2</sub>O<sub>3</sub> catalyst without UV light and gave a degradation percentage of 41.62%, which increased with the addition of UV light. This shows that  $\alpha$ -Fe<sub>2</sub>O<sub>3</sub>-porous ceramic with UV irradiation is the most effective in phenol degradation. In addition, the impregnation of  $\alpha$ -Fe<sub>2</sub>O<sub>3</sub> into porous ceramics demonstrated that porous ceramics prevents the accumulation of  $\alpha$ -Fe<sub>2</sub>O<sub>3</sub> particles, thereby increasing the surface area and photodegradation activity of phenol. The results of phenol photodegradation using the  $\alpha$ -Fe<sub>2</sub>O<sub>3</sub>-porous ceramic adsorption method were more efficient than using a TiO<sub>2</sub>-Fe<sub>2</sub>O<sub>3</sub> photocatalyst conducted by Moradi et al. [55], which reported a 57% phenol degradation from the same initial concentration of 10 mg/L.

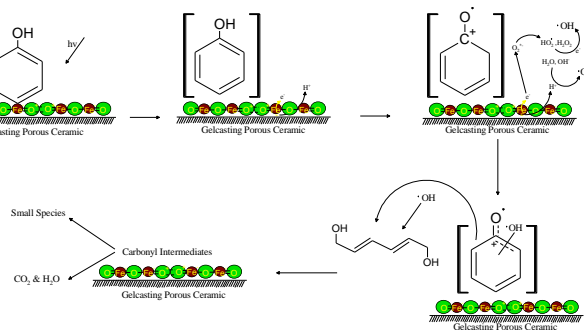


**Figure 7.** The mechanism of phenol photodegradation by  $\alpha$ -Fe<sub>2</sub>O<sub>3</sub> catalyst impregnated on gelcasting porous ceramic

However, the use of nanocomposite photocatalysts, such as AgBr/BiOBr/graphene, BiOCl-TiO<sub>2</sub>, ZnO/Nd-doped BiOBr, and Ag-ZnO, for phenol photodegradation under visible light for 180 min, has reported a degradation of 90% - 97% with an initial concentration of 5 mg/L [56-59]. In addition, phenol degradation has also been carried out using Cu nanoparticles with degradation of 98% [60] and using bioactive carbon (BAC) with 80.5% degradation percent (with an initial concentration of phenol 500 mg/L) [61].

In order to demonstrate the possible practical application of utilizing recycled  $\alpha$ -Fe<sub>2</sub>O<sub>3</sub>-porous ceramic 7% samples (as the best results in photodegradation), a recycling experiment was carried out on the phenol photodegradation process, which is shown in Figure 9. After eight recycling times, the phenol degradation efficiency still maintains >90% performance. This recyclability is higher than the research results before [62]

which uses TiO<sub>2</sub> nanotubes in the degradation of methyl orange dye, with the ability to recycle only 2-3 times. It shows that the new material  $\alpha$ -Fe<sub>2</sub>O<sub>3</sub>-porous ceramic has a wonderful performance of recycling ability in the process of phenol degradation in the environment.

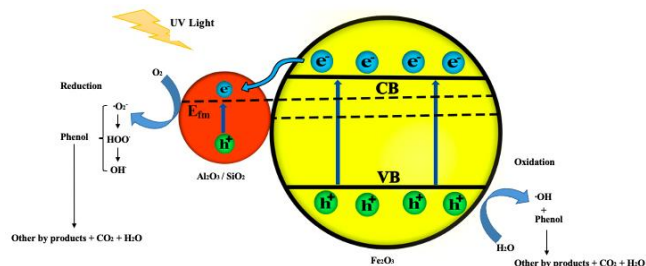


**Figure 8.** Scheme of catalyst activity in degrade phenol

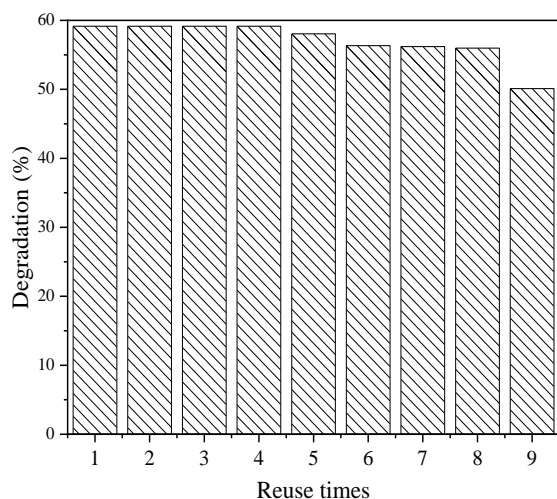


**Figure 9.** Recycle test for the sample  $\alpha$ -Fe<sub>2</sub>O<sub>3</sub>-porous ceramic 7%

#### 4. CONCLUSIONS

The low toxicity gelcasting water-based method with cassava starch concentrations of 1%, 3%, 5%, 7%, and 9% as a pore template has been used in the fabrication of porous ceramics, which is implemented as support for Fe<sub>2</sub>O<sub>3</sub> catalyst in phenol photodegradation. According to the BET analysis results, the cassava starch concentration did not affect the pore character, and a microporous pore was formed. Also, the formation of pores in the ceramic body was observed from the morphology of the SEM analysis, where there was a pore closure after the Fe<sub>2</sub>O<sub>3</sub> catalyst impregnation process. The cassava starch concentration affected the percentage of impregnated Fe<sub>2</sub>O<sub>3</sub> catalyst based on XRD quantitative analysis, with the highest percentage of 41.15% occurring in the ceramic body with 7% starch concentration. In addition, the impregnated Fe<sub>2</sub>O<sub>3</sub> catalyst phase was  $\alpha$ -Fe<sub>2</sub>O<sub>3</sub> with a rhombohedral structure. The highest percentage of phenol degradation was 59.15%, which occurred with the 7% starch concentration. The results obtained are higher than the results of previous studies with the same initial concentration. Based on the recycle test, a new advanced material in this study can be recycled up to 8 times with degradation efficiency still maintains >90% performance.

#### ACKNOWLEDGMENT

This work was supported by Kemenristek/BRIN Indonesia in the scheme of Penelitian Dasar Unggulan Perguruan Tinggi (PDUPT) contract number 109/UN36.11/LP2M/2021 and Lembaga Penelitian dan Pengabdian Masyarakat (LP2M) Universitas Negeri Makassar that has held writing workshops of Scientific Articles in reputable international journals as a forum for the creation of this research article.

#### REFERENCES

- [1] Liu, F., Dong, S., Zhang, Z., et al. (2019). Polyaniline/MWCNT nanocomposite as sensor for electroanalytical determination of phenol in oil field wastewater. *International Journal of Electrochemical Science*, 14: 9122-9131. <https://doi.org/10.20964/2019.09.79>
- [2] US Environmental Protection Agency. (2000). Phenol hazard summary. *Phenol*, 1(1): 95-108.
- [3] On, P., Safety, C. (1982). Titanium: IPCS international programme on chemical safety. World Health Organization, *Environmental Health Criteria*, 24.
- [4] Domacena, A.M.G., Aquino, C.L.E., Balela, M.D.L. (2020). Photo-Fenton degradation of methyl orange using hematite ( $\alpha$ -Fe<sub>2</sub>O<sub>3</sub>) of various morphologies. *Materials Today: Proceedings*, 22: 248-254. <https://doi.org/10.1016/j.matpr.2019.08.095>
- [5] Fernandes, A., Makoś, P., Khan, J.A., Boczkaj, G. (2019). Pilot scale degradation study of 16 selected volatile organic compounds by hydroxyl and sulfate radical based advanced oxidation processes. *Journal of Cleaner Production*, 208: 54-64. <https://doi.org/10.1016/j.jclepro.2018.10.081>
- [6] Ke, Q., Zhang, Y., Wu, X., et al. (2018). Sustainable biodegradation of phenol by immobilized *Bacillus* sp. SAS19 with porous carbonaceous gels as carriers. *Journal of Environmental Management*, 222: 185-189. <https://doi.org/10.1016/j.jenvman.2018.05.061>
- [7] Villegas, L.G.C., Mashhadi, N., Chen, M., Mukherjee, D., Taylor, K.E., Biswas, N. (2016). A short review of techniques for phenol removal from wastewater. *Current Pollution Reports*, 2(3): 157-167. <https://doi.org/10.1007/s40726-016-0035-3>
- [8] Wang, H., Zhang, Z., Jing, M., Tang, S., Wu, Y., Liu, W. (2020). Synthesis of CuNiSn LDHs as highly efficient Fenton catalysts for degradation of phenol. *Applied Clay Science*, 186: 105433. <https://doi.org/10.1016/j.clay.2019.105433>
- [9] Mancipe, S., Tzompantzi, F., Rojas, H., Gómez, R. (2016). Photocatalytic degradation of phenol using MgAlSn hydrotalcite-like compounds. *Applied Clay Science*, 129: 71-78. <https://doi.org/10.1016/j.clay.2016.05.005>
- [10] Wang, J., Xie, T., Han, G., Zhu, Q., Wang, Y., Peng, Y., Yao, Z. (2021). SiO<sub>2</sub> mediated templating synthesis of  $\gamma$ -Fe<sub>2</sub>O<sub>3</sub>/MnO<sub>2</sub> as peroxy monosulfate activator for enhanced phenol degradation dominated by singlet oxygen. *Applied Surface Science*, 560: 149984. <https://doi.org/10.1016/j.apsusc.2021.149984>
- [11] Efavi, J.K., Damoah, L., Bensah, D.Y., Arhin, D.D., Tetteh, D. (2012). Development of porous ceramic bodies from kaolin deposits for industrial applications.

- Applied clay science, 65: 31-36. <https://doi.org/10.1016/j.clay.2012.04.010>
- [12] Ma'Ruf, A., Al Fathoni, M.A.S. (2018). Development of porous ceramic membrane from natural zeolite-clay for microfiltration. In IOP Conference Series: Materials Science and Engineering, 403(1): 012006. <https://doi.org/10.1088/1757-899X/403/1/012006>
- [13] Zouaoui, H., Bouaziz, J. (2017). Physical and mechanical properties improvement of a porous clay ceramic. Applied Clay Science, 150: 131-137. <https://doi.org/10.1016/j.clay.2017.09.002>
- [14] Georgiev, A., Yoleva, A., Djambazov, S. (2018). Influence of brewery waste sludge containing diatomite on the physical properties and thermal conductivity of porous clay bricks. Journal of Chemical Technology and Metallurgy, 53(6): 1117-22.
- [15] Djafar, Z., Suluh, S., Amaliyah, N., Piarah, W.H. (2022). Comparison of the performance of biomass briquette stoves on three types of stove wall materials. International Journal of Design & Nature and Ecodynamics, 17(1): 145-149. <http://dx.doi.org/10.18280/ij dne.170119>
- [16] Zhang, G., Song, A., Duan, Y., Zheng, S. (2018). Enhanced photocatalytic activity of TiO<sub>2</sub>/zeolite composite for abatement of pollutants. Microporous and Mesoporous Materials, 255: 61-68. <https://doi.org/10.1016/j.micromeso.2017.07.028>
- [17] Miao, L., Wu, X., Ji, Z., Zhao, Z., Chang, C., Liu, Z., Chen, F. (2021). Microwave-assisted preparation of porous fibrous ceramic-based catalytic filter elements for the simultaneous removal of NO<sub>x</sub> and dust from high-temperature gases. Separation and Purification Technology, 278: 119549. <https://doi.org/10.1016/j.seppur.2021.119549>
- [18] Rastogi, V.K., Jiang, B., Sturzenegger, P.N., Gonzenbach, U.T., Vetterli, M., Blugan, G., Kuebler, J. (2019). A processing route for dip-coating and characterization of multi-structured ceramic foam. Ceramics International, 45(17): 21887-21893. <https://doi.org/10.1016/j.ceramint.2019.07.199>
- [19] Fan, P.M., Zhen, K.F., Zan, Z.Y., Chao, Z., Jian, Z., Yun, J.Z. (2016). Preparation and development of porous ceramic membrane supports fabricated by extrusion technique. Chemical Engineering Transactions, 55: 277-282. <https://doi.org/10.3303/CET1655047>
- [20] Tabares, E., Cifuentes, S.C., Jiménez-Morales, A., Tsipas, S. A. (2021). Injection moulding of porous MAX phase Ti<sub>3</sub>SiC<sub>2</sub> without using space-holder. Powder Technology, 380: 96-105. <https://doi.org/10.1016/j.powtec.2020.11.022>
- [21] Hotza, D., Nishihora, R.K., Machado, R.A., Geffroy, P.M., Chartier, T., Bernard, S. (2019). Tape casting of preceramic polymers toward advanced ceramics: A review. International Journal of Ceramic Engineering & Science, 1(1): 21-41. <https://doi.org/10.1002/ces2.10009>
- [22] Le Ferrand, H. (2021). Magnetic slip casting for dense and textured ceramics: A review of current achievements and issues. Journal of the European Ceramic Society, 41(1): 24-37. <https://doi.org/10.1016/j.jeurceramsoc.2020.08.030>
- [23] Yang, Z., Chen, N., Qin, X. (2018). Fabrication of porous Al<sub>2</sub>O<sub>3</sub> ceramics with submicron-sized pores using a water-based gelcasting method. Materials, 11(9): 1784. <https://doi.org/10.3390/MA11091784>
- [24] Tian, C., Huang, X., Guo, W., Gao, P., Xiao, H. (2020). Preparation of SiC porous ceramics by a novel gelcasting method assisted with surface modification. Ceramics International, 46(10): 16047-16055. <https://doi.org/10.1016/j.ceramint.2020.03.155>
- [25] Liu, X.Y., Ge, S.T., Zhang, H.J., Bi, Y.B., Jia, Q.L., Zhang, S.W. (2020). Foam-gelcasting preparation of ZrSiO<sub>4</sub> modified porous mullite ceramics. Ceramics-Silikáty, 64(3): 365-370. <https://doi.org/10.13168/cs.2020.0024>
- [26] Putri, S.E., Pratiwi, D.E., Tjahjanto, R.T., Mardiana, D. (2018). On the effect of acrylamide and methylenebisacrylamid ratio on gelcasted ceramic pore character. Journal of Chemical Technology and Metallurgy, 53(5): 841-844.
- [27] Liu, P.F., Li, Z., Xiao, P., Luo, H., Jiang, T.H. (2018). Microstructure and mechanical properties of in-situ grown mullite toughened 3Y-TZP zirconia ceramics fabricated by gelcasting. Ceramics International, 44(2): 1394-1403. <https://doi.org/10.1016/j.ceramint.2017.09.151>
- [28] Luchese, C.L., Spada, J.C., Tessaro, I.C. (2017). Starch content affects physicochemical properties of corn and cassava starch-based films. Industrial Crops and Products, 109: 619-626. <https://doi.org/10.1016/j.indcrop.2017.09.020>
- [29] Nie, Z., Lin, Y. (2015). Fabrication of porous alumina ceramics with corn starch in an easy and low-cost way. Ceramics Silikaty, 59(4): 348-352.
- [30] Wan, W., Huang, C. E., Yang, J., Qiu, T. (2014). Study on gelcasting of fused silica glass using glutinous rice flour as binder. International Journal of Applied Glass Science, 5(4): 401-409. <https://doi.org/10.1111/ijag.12060>
- [31] He, X., Su, B., Zhou, X., et al. (2011). Gelcasting of alumina ceramic using an egg white protein binder system. Ceramics-Silikáty, 55(1): 1-7.
- [32] Lu, Y.J., Ren, B., Wang, C., Rong, Y., Gan, K., Yang, J. L. (2020). Room-temperature gelcasting of alumina with tartaric acid and glutaraldehyde. Ceramics International, 46(8): 11432-11435. <https://doi.org/10.1016/j.ceramint.2020.01.119>
- [33] McArthur, S.L. (2006). Thin films of vanadium oxide grown on vanadium metal. Surface and Interface Analysis, 38(c): 1380-1385. <https://doi.org/10.1002/sia>
- [34] Alag, H.K., Zamel, R.S. (2018). Studying the Properties of Porous Alumina Using Starch as a Binder. Al-Nahrain Journal of Science, 21(3): 112-118. <https://doi.org/10.22401/jnus.21.3.13>
- [35] Putri, S.E., Pratiwi, D.E. (2016). The effect of mole ratio of acrylamide (AM) monomer and methylene-bisacrylamide (MBAM) crosslinker toward the hardness of gelcasting porous ceramics. Proceeding International Conference on Mathematic, Science, Technology, Education and Their Applications, 1(1): 412-415.
- [36] Putri, S.E., Pratiwi, D.E., Triandi, R., Mardiana, D., Side, S. (2018). Performance test of gelcasted porous ceramic as adsorbent of azo dyes. Journal of Physics: Conference Series, 1028(1): 012039. <https://doi.org/10.1088/1742-6596/1028/1/012039>
- [37] Pepper, R.A., Perenlei, G., Martens, W.N., Couperthwaite, S.J. (2021). High purity alumina synthesised from iron rich clay through a novel and selective hybrid ammonium alum process.

- Hydrometallurgy, 204: 105728. <https://doi.org/10.1016/j.hydromet.2021.105728>
- [38] de Leis, C.M., Nogueira, A.R., Kulay, L., Tadini, C.C. (2017). Environmental and energy analysis of biopolymer film based on cassava starch in Brazil. *Journal of Cleaner Production*, 143: 76-89. <https://doi.org/10.1016/j.jclepro.2016.12.147>
- [39] Bengisu, M., Yilmaz, E. (2002). Gelcasting of alumina and zirconia using chitosan gels. *Ceramics International*, 28(4): 431-438. [https://doi.org/10.1016/S0272-8842\(01\)00115-8](https://doi.org/10.1016/S0272-8842(01)00115-8)
- [40] Mohamed, A., Nasser, W.S., Kamel, B.M., Hashem, T. (2019). Photodegradation of phenol using composite nanofibers under visible light irradiation. *European Polymer Journal*, 113: 192-196. <https://doi.org/10.1016/j.eurpolymj.2019.01.062>
- [41] Kagonbé, B.P., Tsozué, D., Nzeukou, A.N., Ngos III, S. (2021). Mineralogical, physico-chemical and ceramic properties of clay materials from Sekandé and Gashiga (North, Cameroon) and their suitability in earthenware production. *Heliyon*, 7(7): e07608. <https://doi.org/10.1016/j.heliyon.2021.e07608>
- [42] Calado, C.M.B., Iturri, M.S., Colonetti, V.C., de Souza, V.C., Fernandes, C.P., Hotza, D., Quadri, M.G.N. (2021). Green production of cellular ceramics by emulsification of sunflower oil followed by gelcasting and starch consolidation. *Journal of Cleaner Production*, 282: 124468. <https://doi.org/10.1016/j.jclepro.2020.124468>
- [43] Offner, A., Bach, A., Sauvart, D. (2003). Quantitative review of in situ starch degradation in the rumen. *Animal Feed Science and Technology*, 106(1-4): 81-93. [https://doi.org/10.1016/S0377-8401\(03\)00038-5](https://doi.org/10.1016/S0377-8401(03)00038-5)
- [44] Talou, M.H., Camerucci, M.A. (2015). Processing of porous mullite ceramics using novel routes by starch consolidation casting. *Journal of the European Ceramic Society*, 35(3): 1021-1030. <https://doi.org/10.1016/j.jeurceramsoc.2014.10.011>
- [45] Liu, Y.F., Liu, X.Q., Wei, H., Meng, G.Y. (2001). Porous mullite ceramics from national clay produced by gelcasting. *Ceramics International*, 27(1): 1-7. [https://doi.org/10.1016/S0272-8842\(00\)00034-1](https://doi.org/10.1016/S0272-8842(00)00034-1)
- [46] de Vargas Brião, G., da Silva, M.G.C., Vieira, M.G.A., Chu, K.H. (2022). Correlation of type II adsorption isotherms of water contaminants using modified BET equations. *Colloid and Interface Science Communications*, 46: 100557. <https://doi.org/10.1016/j.colcom.2021.100557>
- [47] Wang, W., Wang, M., Feng, X., Zhao, W., Luan, C., Ma, J. (2018). Effects of deposition temperature on the structural and optical properties of single crystalline rutile TiO<sub>2</sub> films. *Materials Chemistry and Physics*, 211: 172-176. <https://doi.org/10.1016/j.matchemphys.2018.02.023>
- [48] Alamdari, A., Karimzadeh, R. (2018). Oxidative dehydrogenation of liquefied petroleum gas on copper, zinc and iron oxide impregnated on MFI zeolite assisted by electric power. *Catalysts*, 8(7): 270. <https://doi.org/10.3390/catal8070270>
- [49] Ramadhani, A.N., Abdullah, I., Krisnandi, Y.K. (2022). Effect of Physicochemical Properties of Co and Mo Modified Natural Sourced Hierarchical ZSM-5 Zeolite Catalysts on Vanillin and Phenol Production from Diphenyl Ether. *Bulletin of Chemical Reaction Engineering & Catalysis*, 17(1): 225-239. <https://doi.org/10.9767/bcrec.17.1.13372.225-239>
- [50] Lyubenova, T., Fraga Chiva, D., Carda Castelló, J.B., Kozhukharov, V., Machkova, M.S. (2018). Multifunctional smart coatings on novel ceramics and glassceramic substrates in the context of the circular economy. *Journal of Chemical Technology and Metallurgy*, 53(6): 1103-1116.
- [51] Wang, H.M., Ma, Y.P., Chen, X.Y., Xu, S.Y., Chen, J.D., Zhang, Q.L., Ning, P. (2020). Promoting effect of SO<sub>4</sub><sup>2-</sup> functionalization on the performance of Fe<sub>2</sub>O<sub>3</sub> catalyst in the selective catalytic reduction of NO<sub>x</sub> with NH<sub>3</sub>. *Journal of Fuel Chemistry and Technology*, 48(5): 584-593. [https://doi.org/10.1016/s1872-5813\(20\)30025-6](https://doi.org/10.1016/s1872-5813(20)30025-6)
- [52] Gao, Y., Chiang, F.K., Li, S., Zhang, L., Wang, P., Hensen, E.J. (2021). Influence of hematite morphology on the CO oxidation performance of Au/ $\alpha$ -Fe<sub>2</sub>O<sub>3</sub>. *Chinese Journal of Catalysis*, 42(4): 658-665. [https://doi.org/10.1016/S1872-2067\(20\)63687-7](https://doi.org/10.1016/S1872-2067(20)63687-7)
- [53] GC, S.S., Alkanad, K., Hezam, A., Alsalmeh, A., Al-Zaqri, N., Lokanath, N.K. (2021). Enhanced photo-Fenton activity over a sunlight-driven ignition synthesized  $\alpha$ -Fe<sub>2</sub>O<sub>3</sub>-Fe<sub>3</sub>O<sub>4</sub>/CeO<sub>2</sub> heterojunction catalyst enriched with oxygen vacancies. *Journal of Molecular Liquids*, 335: 116186. <https://doi.org/10.1016/j.molliq.2021.116186>
- [54] Chen, X., Zhang, M., Qin, H., et al. (2022). Synergy effect between adsorption and heterogeneous photo-Fenton-like catalysis on LaFeO<sub>3</sub>/lignin-biochar composites for high efficiency degradation of ofloxacin under visible light. *Separation and Purification Technology*, 280: 119751. <https://doi.org/10.1016/j.seppur.2021.119751>
- [55] Moradi, V., Ahmed, F., Jun, M.B., Blackburn, A., Herring, R.A. (2019). Acid-treated Fe-doped TiO<sub>2</sub> as a high performance photocatalyst used for degradation of phenol under visible light irradiation. *Journal of Environmental Sciences*, 83: 183-194. <https://doi.org/10.1016/j.jes.2019.04.002>
- [56] Sánchez-Rodríguez, D., Medrano, M.G.M., Remita, H., Escobar-Barrios, V. (2018). Photocatalytic properties of BiOCl-TiO<sub>2</sub> composites for phenol photodegradation. *Journal of Environmental Chemical Engineering*, 6(2): 1601-1612. <https://doi.org/10.1016/j.jece.2018.01.061>
- [57] Sin, J.C., Lim, C.A., Lam, S.M., Mohamed, A.R., Zeng, H. (2019). Facile synthesis of novel ZnO/Nd-doped BiOBr composites with boosted visible light photocatalytic degradation of phenol. *Materials Letters*, 248: 20-23. <https://doi.org/10.1016/j.matlet.2019.03.129>
- [58] Singh, P., Raizada, P., Sudhaik, A., Shandilya, P., Thakur, P., Agarwal, S., Gupta, V.K. (2019). Enhanced photocatalytic activity and stability of AgBr/BiOBr/graphene heterojunction for phenol degradation under visible light. *Journal of Saudi Chemical Society*, 23(5): 586-599. <https://doi.org/10.1016/j.jscs.2018.10.005>
- [59] Vaiano, V., Matarangolo, M., Murcia, J.J., Rojas, H., Navío, J.A., Hidalgo, M.C. (2018). Enhanced photocatalytic removal of phenol from aqueous solutions using ZnO modified with Ag. *Applied Catalysis B: Environmental*, 225: 197-206. <https://doi.org/10.1016/j.apcatb.2017.11.075>
- [60] Nayak, R., Ali, F.A., Mishra, D.K., Ray, D., Aswal, V.K., Sahoo, S.K., Nanda, B. (2020). Fabrication of CuO nanoparticle: An efficient catalyst utilized for sensing and degradation of phenol. *Journal of Materials Research*

- and Technology, 9(5): 11045-11059.  
<https://doi.org/10.1016/j.jmrt.2020.07.100>
- [61] Zhao, Z., Li, X., Zeng, X., Zhang, X., Yan, Q. (2020). Preparation of Ti<sub>3</sub>AlC<sub>2</sub> bulk ceramic via aqueous gelcasting followed by Al-rich pressureless sintering. *Journal of the European Ceramic Society*, 40(8): 2878-2886.
- <https://doi.org/10.1016/j.jeurceramsoc.2020.02.028>
- [62] Perillo, P.M., Rodríguez, D.F. (2021). Photocatalysis of Methyl Orange using free standing TiO<sub>2</sub> nanotubes under solar light. *Environmental Nanotechnology, Monitoring & Management*, 16: 100479.  
<https://doi.org/10.1016/j.enmm.2021.100479>